Compact high-efficiency pentahedron and quatrefoil shape antennas with enhanced gain for GSM1800, 3G, 4G-LTE energy harvesting applications

Author for correspondence:
Geriki Polaiah,
E-mail: polaiahgeriki@gmail.com

Geriki Polaiah [iD], K. Krishnamoorthy and Muralidhar Kulkarni

Department of Electronics and Communication Engineering, National Institute of Technology Karnataka Surathkal, Mangalore 575025, India

Abstract

In this paper, three compact, high-efficiency, gain enhanced antennas, and corresponding rectifiers have been proposed for GSM1800, 3G, and 4G-LTE energy harvesting applications. The inverted L-stub is placed on the ground plane of the monopole antenna to get the desired frequency band of GSM1800 MHz. The feed length variation method has been adopted for the slot antennas to obtain the required frequency of 3G and 4G-LTE cellular bands. The performance of antennas is analyzed with the inverted L-stub, feed length variation, and the reflector distance. The maximum gain achieved with the reflector positioned at a distance of $\lambda/4$ from the antenna backside is three times greater than the gain obtained without the reflector. The prototype antennas and rectifiers have been simulated, fabricated, measured various parameters, and compared with the simulation results. The antennas provide more than 82% radiation efficiency and an enhanced gain of greater than 5.6 dB. The peak efficiency of rectifiers of more than 30% has been achieved. The aforementioned three antennas are integrated with their corresponding rectifiers for operating at 1.8, 2.1, and 2.3 GHz frequencies. The proposed rectennas are formidably suitable for the reception of RF power from the cellular bands.

Introduction

The next-generation wireless communication systems demand rectennas for continuous power supply to low power electronic devices, wireless sensors, IoT devices, and biomedical devices. For these devices, providing power continuously with the help of batteries is difficult. Rectennas are an alternative solution for this. There are a lot of applications of rectennas such as radio frequency identification (RFID) tags, wireless charging systems to electric vehicles, space solar power satellites, implantable electronic devices, the ubiquitous power source in emergencies and in-house, smart building. The rectenna is a device consisting of a receiving antenna and rectifier along with an impedance matching network and pass filter. The microwave antenna receives RF energy from the ambient sources and delivers the same to the rectifier circuit for RF to conversion. In this manner, high-frequency RF energy in terms of GHz is converted into energy. The rectenna works according to the principle of conservation of energy in physics which states that "the energy is neither created nor destroyed but converted from one form to another form." The rectenna was first aimed and illustrated by US electrical engineer "William C. Brown" in 1964 and patented in 1969. Recently, several antennas are implemented for operating at the center frequency of GSM900, GSM1800, 3G, and 4G-LTE cellular bands. A wide-band monopole antenna with parasitic strips as described in [1], for mobile phone applications, and dual-band monopole antenna operating at GSM1800 MHz and UMTS2.1 GHz was proposed in [2], for receiving RF power in urban environments. A compact antenna with fractal geometry was also described in [3], for collecting 2.45 GHz frequency signals. An L-probe feeding, dual-port triple-band microstrip patch antenna was reported in [4], for harvesting GSM1800, GSM900, and UMTS2100 RF signals. The ground plane of the fractal loop antenna located inside the loop for GSM1800 MHz cellular band was discussed in [5]. Connecting this type of antenna to the rectifier circuit is difficult. The multi-band reconfigurable antenna for 5G communication cellular bands was suggested in [6]. In [7], a dual-polarized circular patch antenna with the annular slot, stubs, and *V*-shaped slits was reported for UMTS, WLAN, and WiMAX applications. The flexure triangular antenna was presented in [8], for broadband RF energy harvesting from 850 MHz to 1.94 GHz, which covers the GSM900 and GSM1800 bands. A multi-band planar antenna for mobile handset applications was also presented in [9]. A frequency-reconfigurable antenna with the coupled parasitic strip is used to operate a PIN diode as described in [10]. A
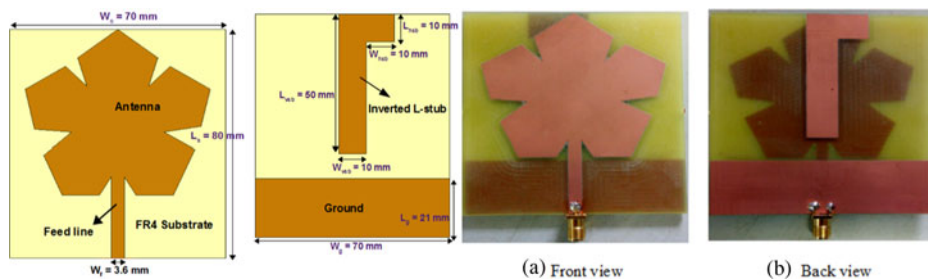
Fig. 1. Antenna geometry and fabricated prototype without the reflector.

wearable fractal geometry EBG structured monopole antenna covers the GSM1800 MHz, and ISM-2.45 GHz bands have been discussed in [11]. A compact multiband antenna was presented in [12], for GSM and LTE mobile phone applications, but the gain of the antenna at the GSM band is low. A dual-polarized broadband antenna with cross-dipole for RF energy harvesting along with the reduction of higher-order harmonics was proposed in [13]. An ink-jet printed multiband antenna has been presented in [14], for flexible devices resonating at the centre frequency of GSM900 MHz and UMTS2.1 GHz bands. In [15], a dual-band polygon shape antenna with a small rectangular slot in opposite faces, and an annular groove in the middle of the patch was described for wearable cellular band applications. A dual-port MIMO rectangular dielectric resonator antenna operating at the frequency of 2.6 GHz for 4G-LTE applications was reported in [16]. A dual broadband antenna with double paired rectangular slit dipoles for 2G, 3G, and 4G mobile applications was described in [17]. The meandered loop quad-band MIMO printed antenna has been proposed in [18] for WiMAX, WLAN, 4G-LTE, and UMTS applications. However, the tetra-band rectennas are reported in [19] and [20] for operating at GSM900, GSM1800, UMTS, and Wi-Fi energy harvesting applications.

In this paper, we propose three compact antennas with high-efficiency, enhanced gain, and integrated with their corresponding rectifiers operating at 1.8, 2.1, and 2.3 GHz cellular bands for ambient RF energy harvesting. The inverted L-stub on the ground plane of the monopole antenna improves the impedance matching. The desired resonant frequency of slot antennas is achieved by varying the feed length without any change in the dimension of the antennas. The enhanced gain is obtained by the use of a reflector at a distance of $\lambda/4$ from the backside of the antenna. The simple transmission line-based L-matching network and Villard voltage doubler are used in the design of the rectifier circuit. The rectifiers have the characteristics of simple structure and easy integration to the antennas, which can be applied for wireless power transfer applications. The rest of this paper is arranged as follows: the detailed design, simulation, and experimental results of antennas and rectifiers are explained in the section "Design details and result analysis of proposed antennas and Design and result analysis of rectifiers." The measurement results of rectennas are shown in the section "Measurement results of proposed rectennas." Finally, conclusions are provided in the section "Conclusion."

Design details and result analysis of proposed antennas

The proposed antennas are designed and simulated by using the CST microwave studio full-wave simulator, fabricated on the FR4 substrate with the characteristics of $\varepsilon_r = 4.3$, tan $\delta = 0.025$, and =

1.6 mm using S103 ProtoMat LPKF PCB machine, and measured using the Agilent Technologies E8363C PNA network analyzer and N9320B spectrum analyzer. The design details, fabricated prototypes, analysis of simulated and measured results of the antennas are described in the following subsections. We propose the following three-antenna designs and result in an analysis for the purpose of energy harvesting.

(i) 1.8 GHz monopole antenna.
(ii) 2.1 GHz slot antenna.
(iii) 2.3 GHz slot antenna.

A 1.8 GHz monopole antenna

The monopole antenna is designed by using the fundamental geometry of the pentahedron. The antenna dimension has been taken to be $80 \times 70 \times 1.6$ mm^3 with the electrical size of the antenna as $0.48\lambda_0 \times 0.42\lambda_0 \times 0.0096\lambda_0$, where "$\lambda_0$" is the free space wavelength at 1.8 GHz. Figure 1 shows the antenna geometry and fabricated prototype without the reflector. The V-shaped slots on the sides of Pentahedron improve the bandwidth of the antenna. However, the inverted L-stub is placed on the ground plane in a suitable position to provide good impedance matching. The 50 Ω feed line is connected to the bottom V-shaped slot of pentahedron that provides maximum power transmission. A high gain antenna is required to receive the low input power from the ambient RF energy sources. For achieving this, single side full metallic reflector at a distance of $\lambda/4$ from the backside of the antenna is used to enhance the gain. When the reflector is placed behind the antenna, the electric fields are added constructively with in-phase at a distance of $\lambda/4$. The back radiation is directed towards the forward direction resulting in an increased gain of the antenna. The side view of the fabricated prototype of the antenna with the reflector is shown in Fig. 2. The dimension of the reflector is $120 \times 120 \times 1.6$ mm^3 and the electrical size is $0.72\lambda_0 \times 0.72\lambda_0 \times 0.0096\lambda_0$. The top antenna is separated from the bottom reflector using Teflon rods of diameter 8 mm.

The reflection coefficient plot of the monopole antenna with and without the inverted L-stub is shown in Fig. 3. A good impedance matching has been obtained at the center frequency and the reflection coefficient bandwidth is not much affected by placing the stub on the suitable position of the ground plane. The measured reflection coefficient bandwidth is 813 MHz. The input impedance of the antenna at 1.8 GHz is 50.6 Ω observed in the Smith chart.

The gain and efficiency plot without the reflector is shown in Fig. 4. The efficiency without the reflector throughout the wideband is more than 82% and the measured gain at center frequency
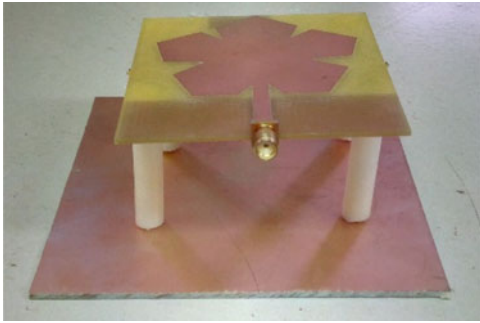
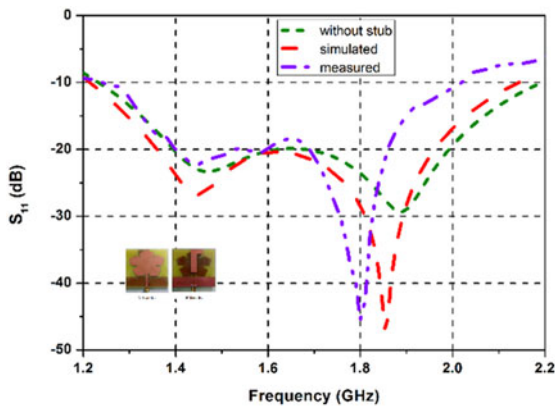**Fig. 2.** Side view of the proposed antenna with the reflector.

Fig. 3. Simulated and measured reflection coefficient with and without the reflector.

is 2.2 dB. The variation of reflection coefficient and gain with the reflector distance is shown in Fig. 5. The reflection coefficient plot is seen to be shifted upwards at a reflector distance of $\lambda/4$. It is observed that consistent gain has been achieved at a reflector distance of $\lambda/4$ from the ground plane from 1.2 to 2.1 GHz wideband frequency. When the distance is increased beyond $\lambda/4$, the reflector and antenna electric fields are not constructively added with each other. It is found that the gain of the antenna is decreased and not stable in the entire wide band.

A 2.1 GHz slot antenna

The quatrefoil shape slot antenna is designed for receiving the UMTS2.1 GHz RF signals. The slot on the ground plane is formed by the connection of four circular slots each of radius 8 mm. The 50 Ω feed line is designed on the backside of the substrate with a width of 3.1 mm for the excitation of the slot. The antenna geometry and fabricated prototype without the reflector are shown in Fig. 6. The dimension of the antenna is $45 \times 40 \times 1.6$ mm^3 and the electrical size is $0.31\lambda_0 \times 0.28\lambda_0 \times 0.0096\lambda_0$, where "$\lambda_0$" is the free space wavelength at 2.1 GHz. The reflector is placed on the backside of the antenna at a distance of $\lambda/4$ to enhance the gain. The side view of the fabricated prototype of a slot antenna with the reflector is shown in Fig. 7. The dimension of the reflector is $62 \times 60 \times 1.6$ mm^3 and the electrical size is $0.43\lambda_0 \times 0.42\lambda_0 \times 0.0096\lambda_0$.

The feed length variation has resulted in the resonant frequency of 2.1 GHz at a feed length of 29.75 mm. Figure 8 denotes the reflection coefficient plot without the reflector. The measured reflection coefficient bandwidth is 253 MHz. Less resonance is observed at lower and higher values of feed lengths throughout the frequency range of 1–10 GHz except for the proposed one. The input impedance of the antenna at 2.1 GHz is 49.2 Ω. Figure 9 illustrates the gain and efficiency plot without the reflector. The radiation efficiency and measured gain at 2.1 GHz are 80% and 1.9 dB, respectively, are obtained. The variation of reflection coefficient and gain with the reflector distance is shown in Fig. 10. The gain of the antenna at $\lambda/4$ distance is higher than other comparison values. The variation of reflector distance does not affect the reflection coefficient bandwidth.

A 2.3 GHz slot antenna

A slot antenna has been designed to operate at 2.3 GHz frequency for the 4G-LTE cellular band. The antenna geometry and fabricated prototype without the reflector are as shown in Fig. 11. The dimension of the antenna is $60 \times 60 \times 1.6$ mm^3 and the electrical size is $0.46\lambda_0 \times 0.46\lambda_0 \times 0.0096\lambda_0$, where "$\lambda_0$" is the free space wavelength at 2.3 GHz. Six circles and one rectangle are used to design the proposed slot. The radius of the left and the right circle is 7 mm. Similarly, the radius of the top two circles and the bottom two circles are 9 mm, respectively. The dimension of the rectangle is 40×28 mm^2. The top and bottom circles are merged with the ground plane. Further, the left and right circles are subtracted from the ground plane to get a required slot. The resonant frequency of 2.3 GHz is obtained at a feed length of 34.5 mm. In addition to this, the reflector is used to obtain an enhancement of the gain at a distance of $\lambda/4$. The dimension of the reflector is $100 \times 100 \times 1.6$ mm^3 and the electrical size is
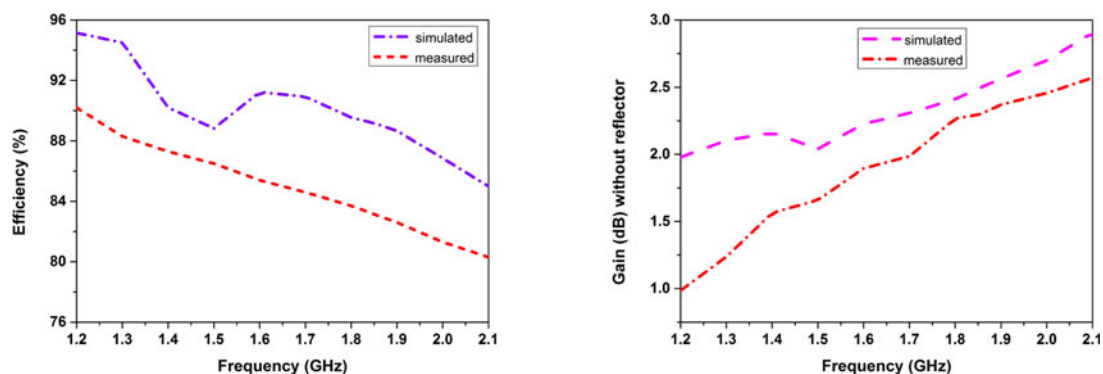

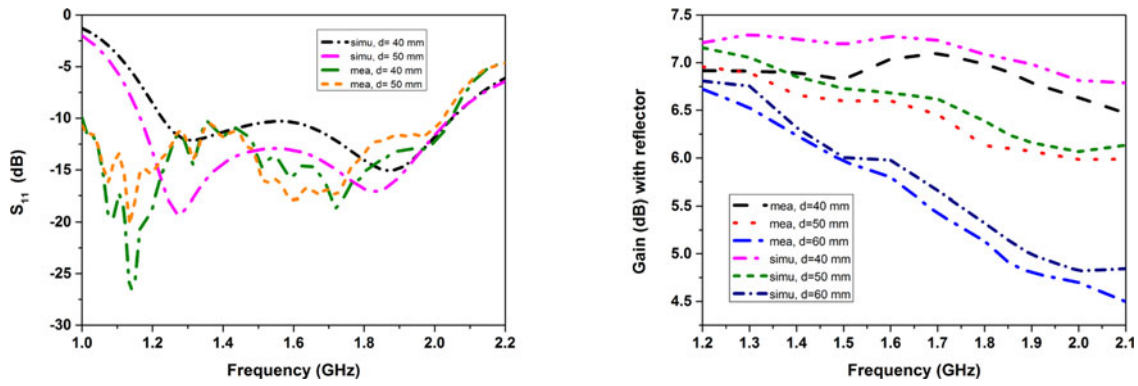**Fig. 4.** Variation of efficiency and gain without the reflector.

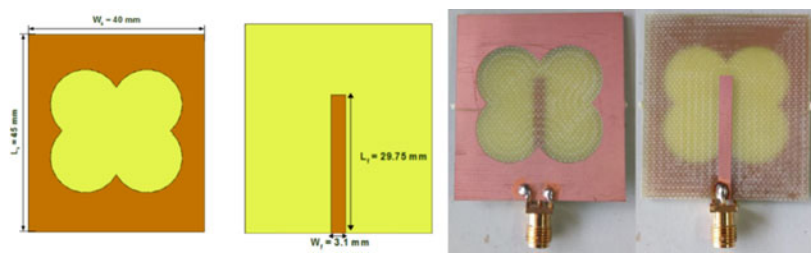**Fig. 5.** Variation of reflection coefficient and gain with the reflector distance.

Fig. 6. Antenna geometry and fabricated prototype without the reflector.

Fig. 7. Side view of the proposed antenna with the reflector.

$0.76\lambda_0 \times 0.76\lambda_0 \times 0.0096\lambda_0$. The side view of the fabricated prototype of the antenna with the reflector is shown in Fig. 12.

The reflection coefficient plot of the proposed slot antenna without the reflector is shown in Fig. 13. The center frequency and bandwidth of the measured reflection coefficient exactly match with the simulation result. The measured reflection coefficient bandwidth is 538 MHz. The input impedance of the antenna at 2.3 GHz is 50.6 Ω. The proposed antenna resonates at the feed length of 34.5 mm. This antenna also resonates at the cellular band frequency of 2.1 GHz and lower WLAN (Wi-Fi) frequency of 2.45 GHz at 36 and 33 mm feed lengths. The gain and efficiency of the antenna without the reflector are shown in Fig. 14. The gain increases on the higher side of the center frequency and the efficiency is also increased. The radiation efficiency and measured gain at 2.3 GHz are 81% and 2.9 dB,
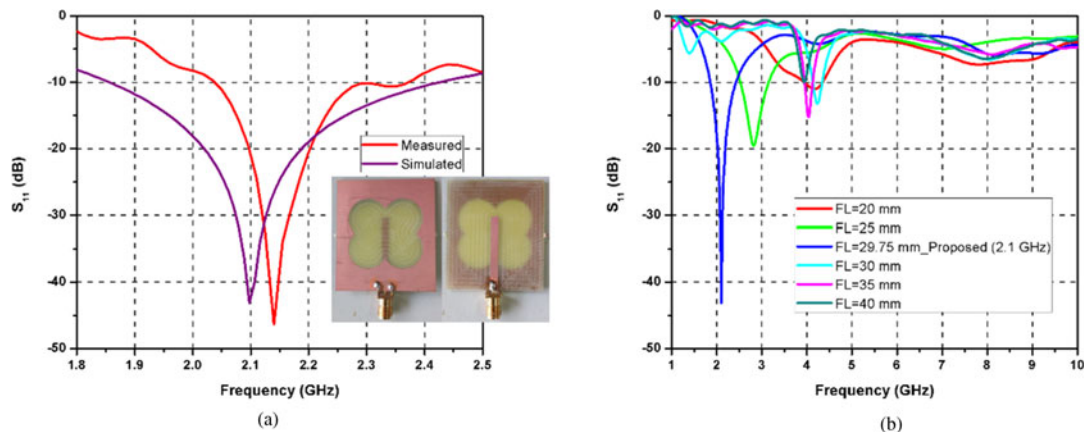

Fig. 8. (A) Simulated and measured reflection coefficient, (B) simulated reflection coefficient at different feed lengths.
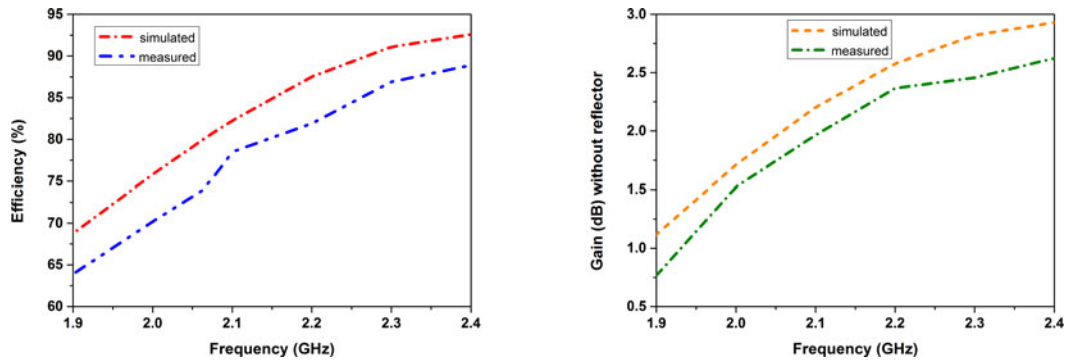
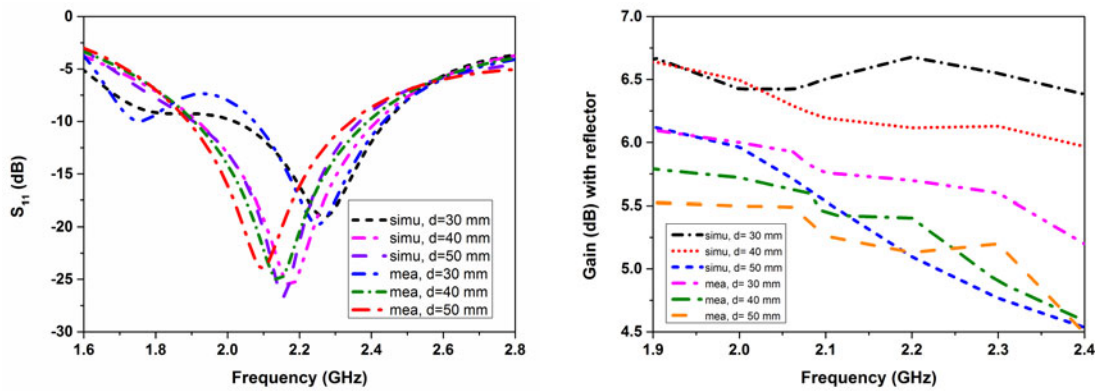**Fig. 9.** Variation of efficiency and gain without the reflector.

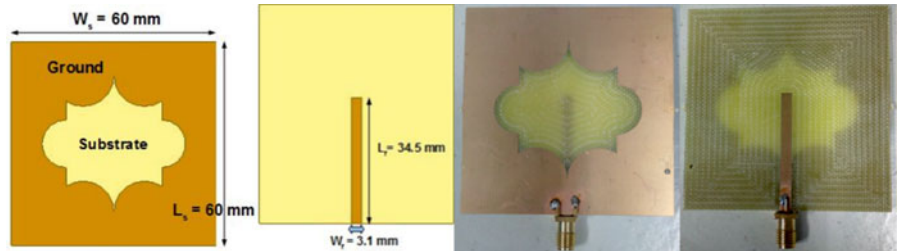**Fig. 10.** Variation of reflection coefficient and gain with the reflector distance.

Fig. 11. Antenna geometry and fabricated prototype without the reflector.
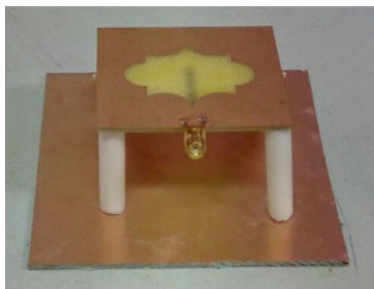

Fig. 12. Side view of the proposed antenna with the reflector.

respectively. The gain and reflection coefficient varies with the reflector distance as shown in Fig. 15. The measured gain of the antenna is 6.8 dB obtained at a reflector distance of $\lambda/4$ and it

maintains the stable value throughout the band. The distance increases beyond $\lambda/4$ and the gain is decreased.

Figure 16 illustrates the comparison between the measured and simulated normalized radiation plots at the two principal planes, *E*-plane (*xz*-plane, $\varphi = 0^0$) and *H*-plane (*yz*-plane, $\varphi = 90^0$) at three distinct frequencies of 1.8, 2.1, and 2.3 GHz of the antennas with the reflector. It can be observed from the radiation patterns that the antennas represent bi-directional radiation along the +*z* and *z*-direction. Similarly, the simulated and measured normalized radiation plots at the two principal planes of the proposed antennas with the reflector at the same frequencies are shown in Fig. 17. The cross-polarization level for the measured and simulated data is less than −20 dB at all three frequencies of the antennas with and without the reflector. It can be seen from the radiation patterns that the proposed antennas with reflector describe the uni-directional radiation along the +*z* direction. In
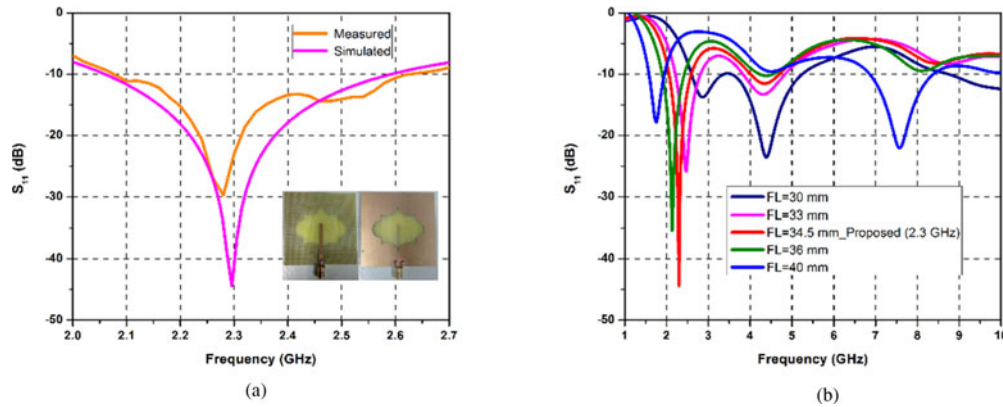
Fig. 13. (A) Simulated and measured reflection coefficient, (B) simulated reflection coefficient at different feed lengths.
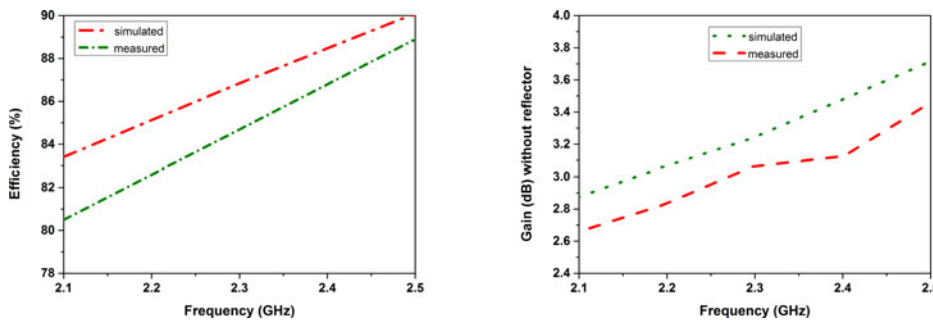

Fig. 14. Variation of efficiency and gain without the reflector.
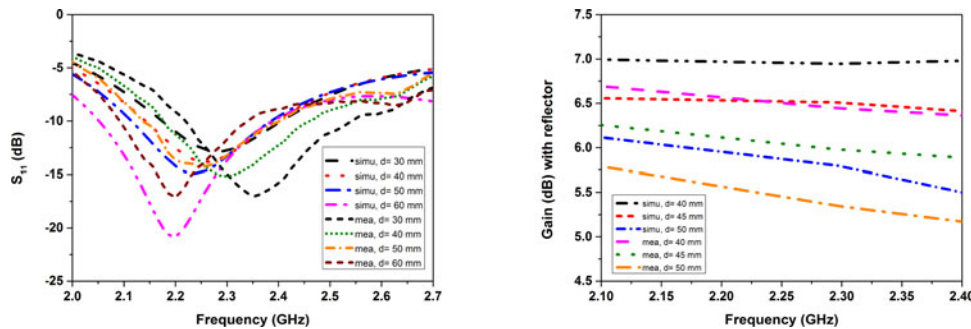

Fig. 15. Variation of reflection coefficient and gain with the reflector distance.

this case, the better front-to-back ratio is achieved at all the frequencies of the proposed antennas. Figure 17 shows the simulated 3D radiation patterns of the antennas with the reflector for all three frequencies. The respective enhanced gains at those frequencies are found to be 7.08, 6.53, and 6.91 dB, respectively. It can be observed that as compared to Figs 4, 9 and 14, the gain increases considerably due to the use of the reflector below the antennas. Besides, a broadside radiation pattern is also generated at an angle of $= 0^0$ at all the three operating frequencies because of this full metallic reflector.

Design and result analysis of rectifiers

The block diagram of a rectifier circuit is shown in Fig. 18. It consists of impedance matching network, voltage doubler (capacitors

$C_1 = C_2 = 100$ pF, diodes D_1 and D_2) and the load resistor $R_L = 3.3$ KΩ. The Schottky diode SMS7630 from Skyworks has been chosen for rectification because it has low threshold voltage $V_f = 148$ mV, junction capacitance under zero bias $C_{j0} = 0.14$ pF, series resistance $R_s = 20$ Ω, and it is useful for low input RF power applications. The SMD capacitors from Murata act as DC blocking before the diode in series connection and DC passing parallel with the load resistor after the diode configuration.

When the positive peak of the RF signal is applied, the diode D_1 is OFF and the diode D_2 is ON, the energy stored in the capacitor C_2. Similarly, when the negative peak of the RF signal is applied, the diode D_1 is ON and the diode D_2 is OFF, the energy stored in the capacitor C_1. Hence, the capacitor C_1 transfers energy to the capacitor C_2 doubling the energy in the capacitor C_2. The input impedance of the rectifier depends on operating
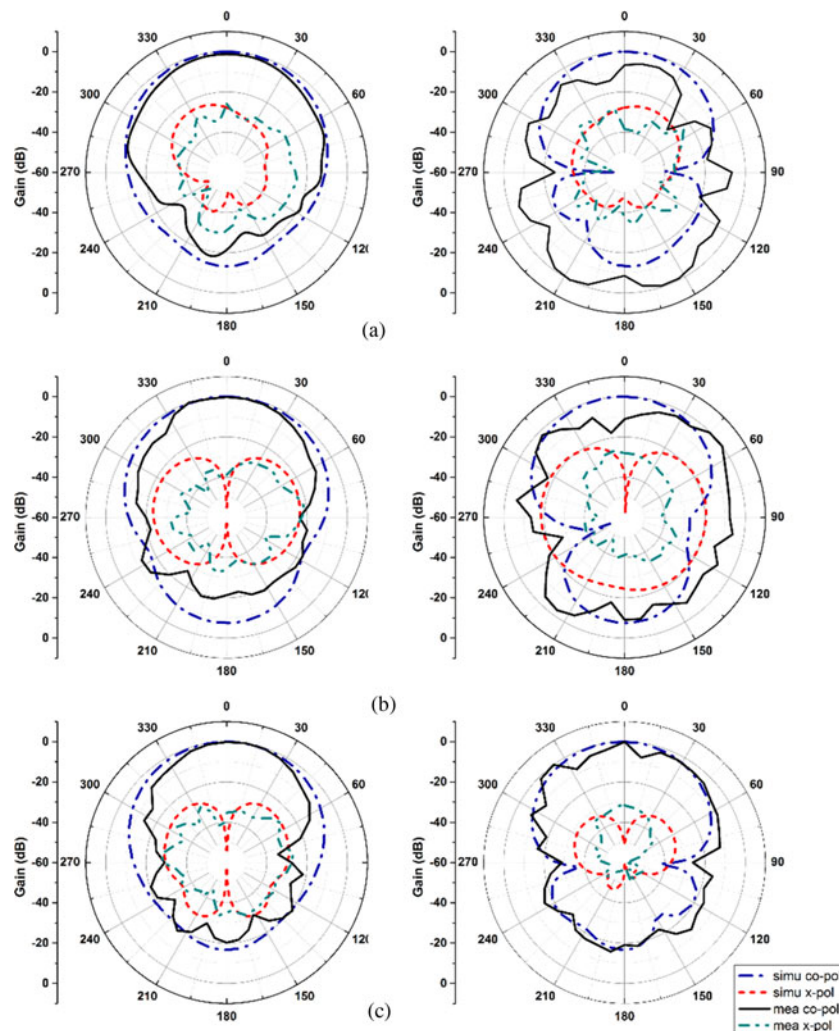
Fig. 16. Simulated and measured 2D radiation patterns of the antennas with the reflector. (A) 1.8 GHz (B) 2.1 GHz (C) 2.3 GHz (left side →*xz*-plane, right side→*yz*-plane).

frequency, input power, and load resistance. Initially, the rectifier without matching network is designed and then the simulation is carried out for the reflection coefficient and input impedance (using Smith chart) by using S-parameter simulation. The input

impedance of rectifiers at 1.8, 2.1, and 2.3 GHz are 18.6-j198.2 Ω, 30.9-j121.9 Ω, and 20.3-j174.2 Ω, respectively.

Further, these impedances have been matched into 50 Ω source impedance by using the Smith chart utility. Finally, the rectifier with a matching network is simulated for the output voltage, and efficiency by using the harmonic balance simulation. The schematic of an impedance matching network for all the three rectifiers operating at 1.8, 2.1, and 2.3 GHz frequencies are shown in Fig. 19. The dimensions of the L-matching network for all three rectifiers are shown in Table 1. The simulated and measured reflection coefficient of the three rectifiers is shown in Fig. 20. The measurement results coincide with the simulated
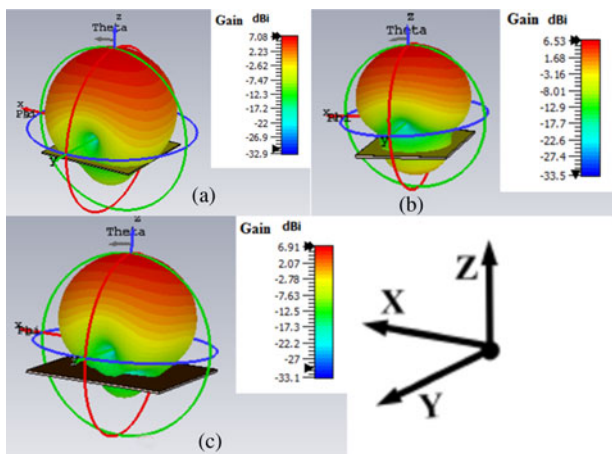

Fig. 17. Simulated 3D radiation patterns of the antennas with the reflector. (A) 1.8 GHz (B) 2.1 GHz (C) 2.3 GHz.
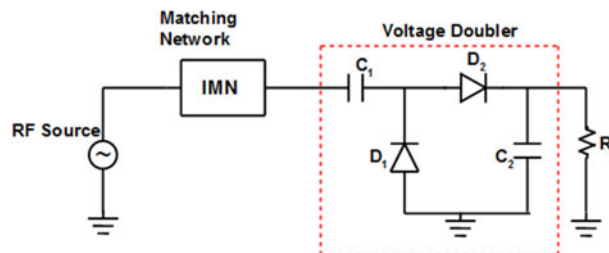

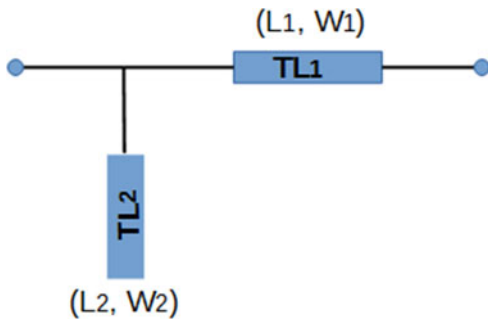**Fig. 18.** Block diagram of a rectifier circuit.

Fig. 19. Impedance matching network for the proposed three rectifiers.

Table 1. Dimensions of the L – matching network of three rectifiers (unit: mm)

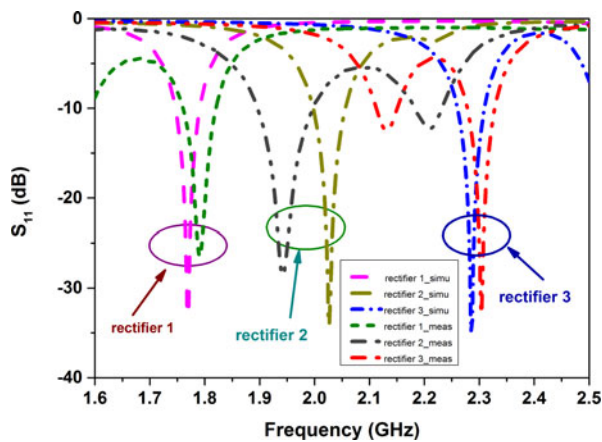| 1.8 GHz rectifier	2.1 GHz rectifier	2.3 GHz rectifier
$L_1 = 22.1$, $W_1 = 3.1$	$L_1 = 19.2$, $W_1 = 3.1$	$L_1 = 17$, $W_1 = 3.1$
$L_2 = 20.3$, $W_2 = 3.1$	$L_2 = 15.4$, $W_2 = 3.1$	$L_2 = 17.8$, $W_2 = 3.1$

Fig. 20. Simulated and measured reflection coefficient of the three rectifiers.
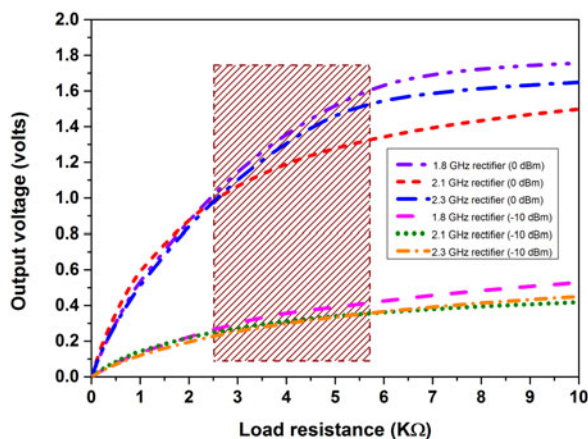

Fig. 21. Simulated output voltage versus load resistance of the rectifiers at different input power levels.
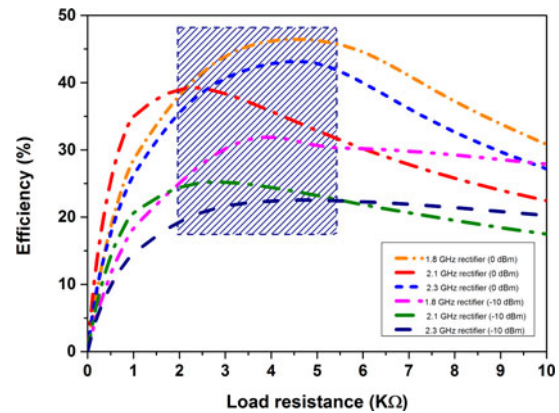

Fig. 22. Simulated efficiency versus load resistance of the rectifiers at different input power levels.

ones with a small deviation due to the fabrication tolerances and soldering of the diodes, capacitors, and via grounds. The optimization of load resistance is essential for the analysis of the rectifier circuit because the output voltage and efficiency depend on load resistance. The efficiency of the rectifier is determined by using equation (1), as given below.

$$\text{Efficiency (\%)} = \frac{V_0^2}{R_L} \times \frac{1}{P_{in}} \times 100 \,. \tag{1}$$

The change in voltage and efficiency for the load resistance at different input power levels of 0 dBm and −10 dBm are shown in Figs 21 and 22. Simulated output voltage versus input power of the rectifiers at different load resistance values is shown in Fig. 23. The maximum voltage and efficiency are obtained in the range of 2 KΩ to the 5 KΩ load resistance. The optimized fixed load resistance has been chosen as 3.3 KΩ within that range. The output voltage and efficiency versus input power of the rectifiers at 3.3 KΩ load resistance are as shown in Figs 24 and 25. The output voltage is almost similar at the three frequencies within the input power range of −30 to 15 dBm. The maximum efficiency is obtained at an input power of 0 dBm (1 mW) for all the frequencies. The design and simulations are performed using the Keysight Technologies Advanced Design System. The three rectifiers are fabricated on the Rogers RO4003C substrate with the characteristics of $\varepsilon_r = 3.38$, tan $\delta = 0.0027$, and $t = 1.52$ mm. The fabrication prototypes of proposed rectifiers for experimental validation are shown in Fig. 26. These rectifiers can be directly integrated into the corresponding proposed antennas for the rectennas design. Similarly, the output voltage of the rectennas can also be measured by satisfying the far-field distance between transmit and receive antennas from which the efficiency of rectennas has been calculated.

Measurement results of proposed rectennas

The measurement system of a proposed 1.8 GHz monopole rectenna is shown in Fig. 27. The RF signal generator N9310A (9 KHz–3 GHz) from Agilent Technologies is connected to the transmitting antenna for transmitting RF energy. A standard double ridged broadband transmitting horn antenna has varying gain from 3–16 dB in 0.8–18 GHz range of frequency is used for the
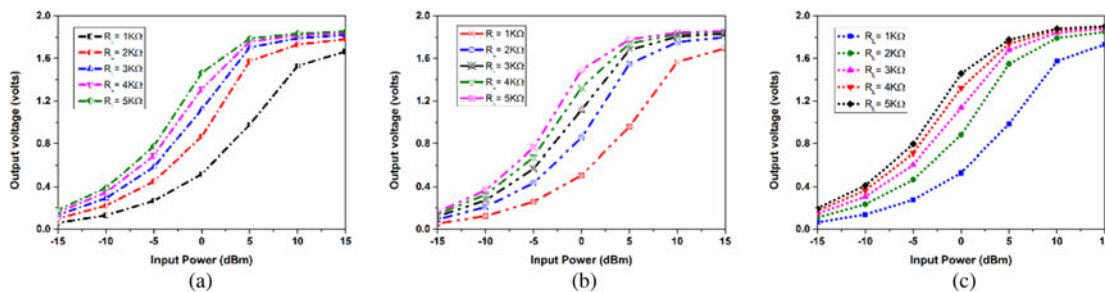
Fig. 23. Simulated output voltage versus input power of the rectifiers at different load resistance values (a) 1.8 GHz (b) 2.1 GHz (c) 2.3 GHz.
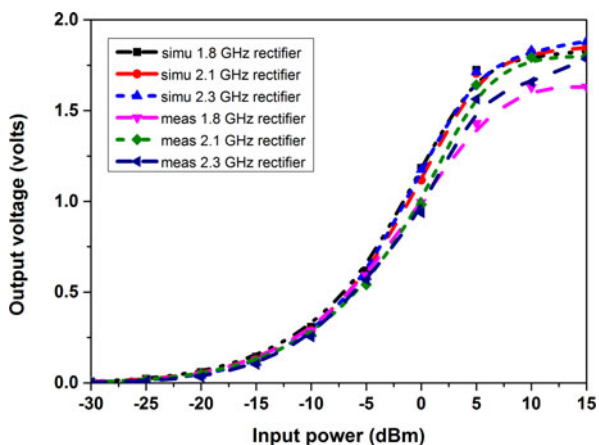

Fig. 24. Simulated and measured output voltage versus input power of the rectifiers at 3.3 KΩ load resistance.

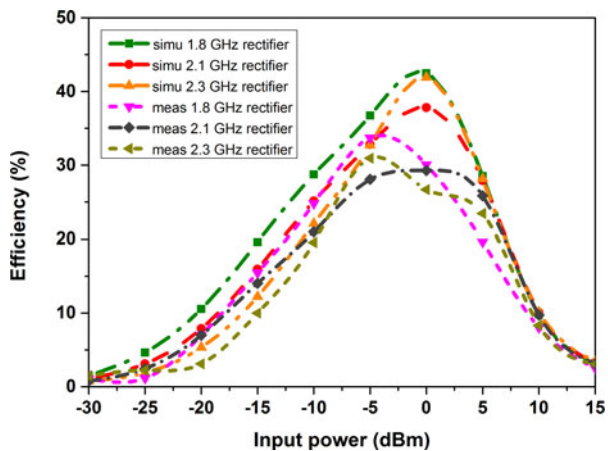**Fig. 26.** Fabrication prototypes of the proposed rectifiers.

Fig. 25. Simulated and measured efficiency versus input power of the rectifiers at 3.3 KΩ load resistance.

measurement of rectenna. The distance between transmitting antenna and rectenna has been chosen such that the far-field condition is valid for 1.8 GHz operating frequency. The power received by the receiving antenna is measured using the Agilent Technologies N9320B (9 KHz–3 GHz) spectrum analyzer. The distance is increased gradually by 0.2 m greater than the far-field distance and measure the received power at different distances. The rectifier is connected to an antenna in the position of a
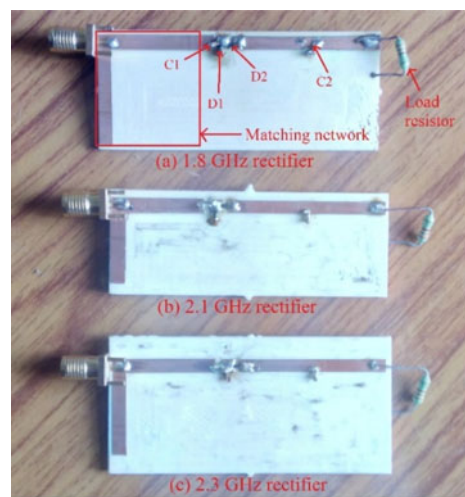
spectrum analyzer. The output voltage is measured using the multimeter at similar distances at which the received power was measured. The RF– conversion efficiency of rectenna using corresponding output voltage, input power, and load resistance of 3.3 KΩ can be calculated using equation (1). The experiments are carried out with a similar procedure (as mentioned above) for the measurement of 2.1 and 2.3 GHz rectennas and efficiencies are calculated for RF power received by the input of antennas and output voltages. The conversion efficiency of the rectennas with respect to the received RF power at the input of the antennas is plotted in Fig. 28. The proposed 1.8 GHz monopole rectenna mounted on a chamber in receiving mode for the measurement of the output voltage is shown in Fig. 29. The summary of proposed antennas with different parameters and geometry details are listed in Table 2.

Similarly, the comparison with the reported rectennas is also listed in Table 3. The proposed antennas possess good gain at the operating frequencies of 1.8, 2.1, and 2.3 GHz. A lot of RF power is available in the environment through cell towers, Wi-Fi routers, etc., but at a low level. To receive low-level RF power, high gain antennas are essential. The high gain antennas effectively receive low input RF power from the ambient sources. The proposed antennas have a gain of more than 5.6 dB and better than [2, 3, 5, 13]. The proposed rectennas indicate higher efficiency at a low input power of −20 dBm compared to [4, 19, 20]. The power management unit (PMU) is connected to the rectenna instead of a load resistor in [19].
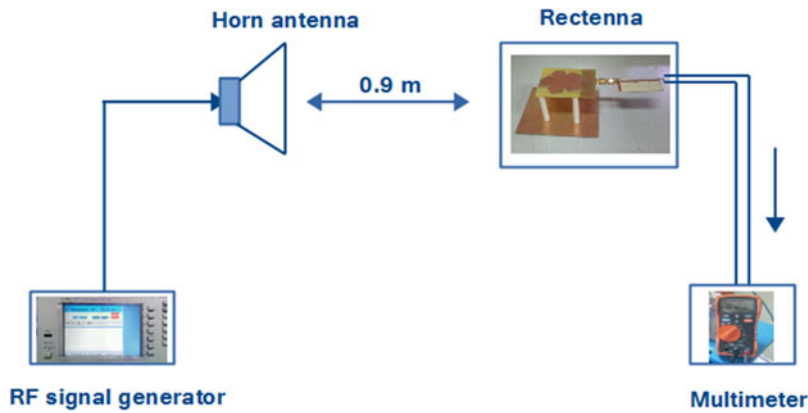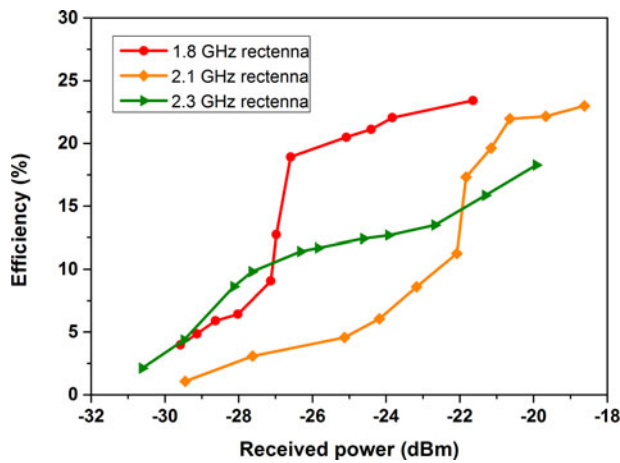
Fig. 27. Measurement system of the rectenna.

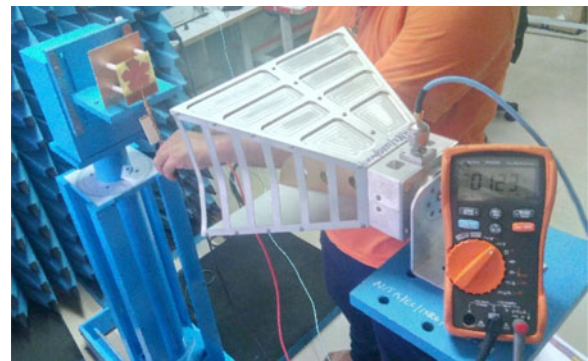**Fig. 28.** Measured efficiency of the rectennas for the received RF power at the input of antennas.

Fig. 29. Measurement of a 1.8 GHz monopole rectenna mounted on a chamber in receiving mode.

Table 2. Summary of proposed antennas

Antenna parameters and geometry details	Antenna-1	Antenna-2	Antenna-3
Cellular band	GSM1800	3G	4G-LTE
Center frequency (GHz)	1.8	2.1	2.3
Radiation efficiency (%)	89	83	87
−10 dB bandwidth (MHz) simulated and measured	928 and 813	568 and 253	552 and 538
Gain without reflector (dB) simulated & measured	2.5 and 2.2	2.2 and 1.9	3.2 and 3.1
Gain with reflector (dB) simulated and measured	7.1 and 6.9	6.5 and 5.7	6.9 and 6.8
Antenna size (mm^3)	80 × 70 × 1.6	45 × 40 × 1.6	60 × 60 × 1.6
Antenna size (λ_o^3)	0.48 × 0.42 × 0.0096	0.31 × 0.28 × 0.0096	0.46 × 0.46 × 0.0096
Reflector size (mm^3)	120 × 120 × 1.6	62 × 60 × 1.6	100 × 100 × 1.6
Reflector size (λ_o^3)	0.72 × 0.72 × 0.0096	0.43 × 0.42 × 0.0096	0.76 × 0.76 × 0.0096

Where "λ_o" is the free-space wavelength at the center frequency of the antenna.

Conclusion

In this paper, three compact high-efficiency rectennas with enhanced gain working in GSM1800, 3G, and 4G-LTE frequency bands have been proposed for RF energy harvesting applications. The dimension of the monopole antenna is not changed. However, the inverted L-stub and ground plane are optimized for resonating at the desired frequency of 1.8 GHz. Similarly, the ground plane and dimension of slot antennas are not altered but the feed length has been varied for resonating at the 2.1, and 2.3 GHz desired frequencies. The input impedance of the antennas at these frequencies is maintained at 50 Ω. The high peak

Table 3. Comparison with the reported rectennas

Ref.	Frequency (GHz)	S_{11} band width (MHz)	Size ^{a} (mm)	Size ^{a} (λ_0)	Gain (dB)	Antenna efficiency (%)	Rectenna efficiency (%)	Optimal load (KΩ)
[2]	Dual band 1.8, 2.1	2100	130×80	0.78×0.47	3.6, 3.8	NM	45, 33 at −7 dBm	0.9, 1.5
[3]	Single band 2.45	118	35×35	0.28×0.28	0.5	34	47 at −10 dBm	3.3
[4]	Triple band 0.9, 1.8, 2.1	30, 400	284×175	0.62×0.54	8.1, 7.1, 8.1	NM	27.3, 20, 14 at −20 dBm	5
[5]	Single band 1.8	110	45×45	0.27×0.27	3.0	NM	25 at −20 dBm	12
[13]	Broad band 1.8–2.5	700	70×70×13.2	0.42×0.42	4.1	NM	32 at −20 dBm	14.7
[19]	Multiband 0.9, 1.75, 2.15, 2.45	20, 124, 367	155×155×7.2	1.12×1.12×0.052	9.8, 5.0, 4.8, 9.6	NM	16 at −10 dBm	PMU
[20]	Multiband 0.9, 1.8, 2.1, 2.4	126, 105, 158, 93	100×100	0.59×0.59	5.8, 5.2, 5.3, 6.1	NM	15 at −20 dBm	11
This work	Single band 1.8	928	183×120×42	1.08×0.72×0.25	6.9	89	23 at −21 dBm	3.3
	Single band 2.1	568	136×62×36	0.95×0.43×0.26	5.7	83	22 at −19 dBm	3.3
	Single band 2.3	552	167×100×33	1.28×0.76×0.24	6.8	87	17 at −20 dBm	3.3

NM, not mentioned; PMU, power management unit.
Where "λ_0" is the free-space wavelength at the center frequency of the antenna.
^{a}Unit mm²/λ_0^2 for 2-dimension and mm³/λ_0^3 for 3-dimension rectennas.

gains are obtained by using the full copper patch reflector. The measured gains of antennas at those frequencies are 6.9, 5.7, and 6.8 dB, respectively. The three rectifiers along with matching circuits have been separately designed, fabricated, and measured to achieve the desired performance. The proposed antennas have finally been integrated with the rectifiers to accomplish the rectennas. These rectennas are used to receive the low input RF power from the ambient sources of cellular bands.

References

1. **Tang R and Du Z** (2017) Wideband monopole without lumped elements for octa-band narrow frame TE smartphone. *IEEE Antennas and Wireless Propagation Letters* **16**, 720–723.
2. **Khemar A, Kacha A, Takhedmit H and Abib G** (2018) Design and experiments of a dual-band rectenna for ambient RF energy harvesting in urban environments. *IET Microwaves Antennas and Propagation* **12**, 49–55.
3. **Chuma EL, Lano Y, Bravo-Roger LL, De la Torre Rodríguez LM and Sanchez-Soriano MA** (2018) Compact rectenna based on a fractal geometry with a high conversion energy efficiency per area. *IET Microwaves Antennas and Propagation* **12**, 173–178.
4. **Shen S, Chiu CY and Murch RD** (2017) A dual-port triple-band L-probe microstrip patch rectenna for ambient RF energy harvesting. *IEEE Antennas and Wireless Propagation Letters* **16**, 3071–3074.
5. **Zhang M, Andrenko AS, Liu X, Li Z and Tan HZ** (2017) A compact fractal loop rectenna for RF energy harvesting. *IEEE Antennas and Wireless Propagation Letters* **16**, 2424–2427.
6. **Trinh LH** (2016) Reconfigurable antenna for future spectrum reallocations in 5G communications. *IEEE Antennas and Wireless Propagation Letters* **15**, 1297–1300.
7. **Mathew S, Ameen M, Jayakrishnan MP, Mohanan, P and Vasudevan, K** (2016) Compact dual polarised V slit, stub, and slot embedded circular patch antenna for UMTS/WiMAX/WLAN applications. *Electronic Letters* **52**, 1425–1426.
8. **Arrawatia M, Baghini MS and Kumar G** (2016) Broadband bent triangular omnidirectional antenna for RF energy harvesting. *IEEE Antennas and Wireless Propagation Letters* **16**, 36–39.
9. **Cui Y, Yang L, Liu B and Li RL** (2016) Multiband planar antenna for LTE/GSM/UMTS and WLAN/WiMAX handsets. *IET Microwaves Antennas and Propagation* **10**, 502–506.
10. **Bhellar B and Tahir FA** (2015) Frequency reconfigurable antenna for handheld wireless devices. *IET Microwaves Antennas and Propagation* **9**, 1412–1417.
11. **Velan S, Sundarsingh EF, Malathi K, Sarma, AK, Raviteja, C, Sivasamy, R and Jayaram, KP** (2015) Dual-band EBG integrated monopole antenna deploying fractal geometry for wearable applications. *IEEE Antennas and Wireless Propagation Letters* **14**, 249–252.
12. **Chou YJ, Lin GS, Chen JF, Chen, LS and Houng, MP** (2015) Design of GSM/LTE multiband application for mobile phone antennas. *Electronic Letters* **51**, 1304–1306.
13. **Song C, Huang Y, Zhou J, Zhang J, Yuan, S and Carter, P** (2015) A high-efficiency broadband rectenna for ambient wireless energy harvesting. *IEEE Transactions on Antennas and Propagation* **63**, 3486–3495.
14. **Ahmed S, Tahir FA, Shamim A and Cheema HM** (2015) A compact Kapton-based inkjet-printed multiband antenna for flexible wireless devices. *IEEE Antennas and Wireless Propagation Letters* **14**, 1802–1805.
15. **Sundarsingh EF, Sangeetha V, Malathi K, Sarma AK, Raviteja, C and Alsath, MGN** (2014) Polygon-shaped slotted dual-band antenna for wearable applications. *IEEE Antennas and Wireless Propagation Letters* **13**, 611–614.
16. **Roslan SF, Kamarudin MR, Khalily M and Jamaluddin MH** (2014) A MIMO rectangular dielectric resonator antenna for 4G applications. *IEEE Antennas and Wireless Propagation Letters* **13**, 321–324.

17. **Cui Y, Li RL and Wang P** (2013) Novel dual-broadband planar antenna and its array for 2G/3G/LTE base stations. *IEEE Transactions on Antennas and Propagation* **12**, 1132–1139.

18. **Fernandez SC and Sharma SK** (2013) Multiband printed meandered loop antennas with MIMO implementations for wireless routers. *IEEE Antennas and Wireless Propagation Letters* **12**, 96–99.

19. **Masotti D, Costanzo A, Prete MD and Rizzoli V** (2013) Genetic-based design of a tetra- band high-efficiency radio-frequency energy harvesting system. *IET Microwaves Antennas and Propagation* **7**, 1254–1263.

20. **Kuhn V, Lahuec C, Seguin F and Person C** (2015) A multi-band stacked RF energy harvester with RF-to-DC efficiency up to 84%. *IEEE Transactions On Microwave Theory and Techniques* **63**, 1768–1778.

Geriki Polaiah received the B.Sc. and M.Sc degrees in Physics with specialization in Electronics from Sri Venkateswara University, Tirupati, India, in 2005 and 2007 and the M.Tech. Degree in Electronics and Communication Engineering from Jawaharlal Nehru Technological University, Anantapur, India, in 2010. He is currently pursuing a Ph.D. degree with the National Institute of Technology Karnataka Surathkal, Mangalore, India. His current research interests include antennas and rectifier circuits for RF energy harvesting and wireless power transfer applications.

Krishnamoorthy. K received the B.E. degree in Electronics and Communication Engineering from Bharathiar University, Coimbatore, India, in 2002, and the M.E. degree in Communication Systems from Anna University, Chennai, India, in 2007 and the Ph.D. degree in electrical engineering from IIT Bombay, Mumbai, India, in 2016. He worked as a member of technical staff in HCL Technologies, India and a deputy engineer, BEL, Bangalore, India. Currently, he has been working as an Assistant Professor in the Department of Electronics and Communication Engineering, NITK Surathkal, Mangalore, India. His current research interests include antenna design, meta-materials, reconfigurable and multiband antenna design, and RF & Microwave Engineering and Metasurfaces.

Muralidhar Kulkarni received his B.E. degree in Electronics Engineering from University Visvesvaraya College of Engineering, Bangalore, India, and the M.Tech degree in Satellite Communication and Remote Sensing from IIT Kharagpur, Kharagpur, India, and the Ph.D. degree in Electronics & Communication Engineering from JMI Central University, New Delhi, India. Prof. Kulkarni is a Senior Member of IEEE, Fellow of the IETE, Life Member of ISTE, Life Member of Computer Society of India, and a Member of Board of Governors, NITK Surathkal, India. He worked as an Aeronautical Engineer, Helicopter Design Bureau, Hindustan Aeronautics Limited (HAL), Bangalore. Currently, he has been working as a Senior Professor (HAG) in the Dept. of Electronics & Communication Engineering, NITK Surathkal, Mangalore, India. His current research interests include Digital Communication and Networks, WSNs and Antenna Design using metamaterials.